Journal of Materials Chemistry A

COMMUNICATION

View Article Online
View Journal | View Issue

Cite this: J. Mater. Chem. A, 2015, 3, 16424

Received 30th May 2015
Accepted 13th July 2015

DOI: 10.1039/c5ta03917g

www.rsc.org/MaterialsA

Highly rate and cycling stable electrode materials constructed from polyaniline/cellulose nanoporous microspheres†

Dingfeng Xu,‡[a] Xu Xiao,‡[b] Jie Cai,[a] Jun Zhou*[b] and Lina Zhang*[a]

To resolve the problem of the pulverization and rapid capacity fading of polymer electrodes, novel electrode materials were constructed from polyaniline/cellulose microspheres (PANI/CM), which were fabricated *via in situ* synthesis of PANI on cellulose matrix by using phytic acid (PA) as a "bridge", for the first time. The constructing of the PANI/PA/CM successfully resolved the problem of the pulverization of PANI to be used as electrode materials. In our findings, the PANI subparticles with nanomesh structure were dispersed homogeneously in the cellulose microspheres from inside to outside, as a result of the firm connection between the hydrophobic PANI and the hydrophilic cellulose through the PA "bridge" to create micro- and nano-porous architecture. Meanwhile, the other parts of PANI deposited on the surface of the microspheres to form a loose coralline structure, leading to the ion channels for the electrolyte penetration. The PANI/PA/CM composite electrodes exhibited excellent cycling stability (over 12 000 cycles) and high rate capability, showing great potential for use in energy-storage devices.

Faced with the impending energy crisis, research on high efficiency, low cost, environmentally friendly, and renewable energy resources has attracted much attention.[1] Electrochemical capacitors, also known as supercapacitors (SCs), have significant potential as energy storage devices due to their unique properties, which include but are not limited to high power density, long cycle life, fast charge/discharge rates, and low manufacturing costs.[2] Conductive polymers, such as polyaniline (PANI), polypyrrole (PPy), and their derivatives, are commonly used as pseudocapacitive electrode materials owing to their facile synthesis, flexibility in processing and displaying high capacitance value.[3] However, the cycling performance of PANI is poor due to the large volumetric swelling and shrinking during the charge/discharge process as a result of ion doping and dedoping.[4] Thus, a number of efforts have centred on improving their cycling stability, such as adding of the graphene composite,[5] carbon nanotubes (CNT)[6] and hybrid with or electrochemically deposited onto transition metal oxides to achieve high-performance hybrid electrode materials.[7] The pulverization of PANI and rapid capacity fading of the polymer electrodes and their imperfect preparation, including being hazardous, time-consuming, or high cost, limit their widespread application. Therefore, a deep development of high rate and cycling stable electrode materials *via* relatively simple, cost-effective, and green approaches is essential for their successful application.

It is worth noting that the theme of the spring 2015 ACS National Meeting was "Chemistry of Natural Resources". Cellulose is the most abundant renewable resource on earth, and also one of the most intransigent macromolecules with moderate thermal stability.[8] Cellulose and its derivatives have been applied to many aspects, such as catalyst supports, electronics and biomaterials, where cellulose's structure and properties have been thought to be very important.[9] Moreover, bacterial cellulose has also been used as a support to fabricate conductive polymer/cellulose composites,[10] and PANI/cellulose functional materials, such as films, hydrogels and fibers, have been fabricated from PANI/cellulose solution in NaOH/urea aqueous solution in our laboratory.[11] Furthermore, cellulose/Fe_3O_4 microspheres and cellulose/TiO_2 microspheres have been constructed by using cellulose microspheres, which were prepared from cellulose solution in an NaOH/urea system, as a template *via in situ* synthesis or by blending.[12] Additionally, cellulose/PPy aerogels[13] and PANI/cellulose films[14] have been fabricated by using cellulose hydrogels as a template *via in situ* synthesis. However, these materials could not simultaneously fulfill the requirements of electrochemical properties and cycling performance for energy-storage applications. Cui *et al.* have reported that natural phytic acid (PA) has phosphorus

[a]College of Chemistry & Molecule Sciences, Wuhan University, Wuhan, 430072, China. E-mail: zhangln@whu.edu.cn

[b]Wuhan National Laboratory for Optotelectronics, School of Optical and Electronic Information, Huazhong University of Science and Technology, Wuhan, 430074, China. E-mail: jun.zhou@mail.hust.edu.cn

† Electronic supplementary information (ESI) available. See DOI: 10.1039/c5ta03917g

‡ These authors contributed equally to this work.

oxygen groups,[15] which can form strong hydrogen-bonding with polyaniline to obtain excellent electrochemical activity materials. It is not hard to imagine that PA can also form hydrogen-bond with cellulose chains, thus it can create a "bridge" to simultaneously cross-link both PANI and cellulose, similar to a "calcium bridge" in ionically crosslinked alginate.[16] Additionally, the *in situ* polymerization can further result in the cross-linking the phytic acid "bridge" with aniline monomers to create a mesh-like PANI in the cellulose microspheres. Thus, constructing PANI/cellulose microspheres can resolve the problem of the pulverization.

Herein, for the first time, we demonstrated a large-scale and efficient strategy to construct hydrogen-bonding-stabilized polyaniline/cellulose nanoporous structure microspheres using phytic acid as a "bridge", which was used as a pseudocapacitance electrode material. The cellulose was dissolved in 4.6 wt% LiOH/15 wt% urea aqueous system with cooling, which dissolves cellulose more easily than NaOH/urea aqueous solution.[17] The resulted cellulose solution was dropped into Span 85 in isooctane with stirring *via* emulsifier to fabricate regenerated cellulose microspheres (CM). Subsequently, *in situ* polymerization of aniline monomer occurred in the cellulose matrix in the presence of phytic acid to obtain large scale products of the polyaniline/cellulose nanoporous microspheres (Fig. S1†). Fig. 1a–d shows the SEM images of the CM and their size distribution. The CM microspheres with relatively narrow size distribution from 1 to 9 μm exhibited homogeneous porous structure with pore size ranging from about 100 to 200 nm, which was very useful as a micro-reactor for the polymerization of PANI. Fig. 1e and h shows SEM images of the PANI/PA/CM and their size distribution. Obviously, the PANI with coralline pattern appeared on the surface of the CM, where the unlimited space induced the rapid growing of the PANI aggregates to form loose structure with micro- and nano-pores, as a result of the unique role of attraction and repulsion of the hydrophilic phytic acid hydrogen bonded on the hydrophilic PANI chains. Thus, the size of the PANI/PA/CM was larger than that of CM, and the PANI/PA/CM exhibited a rough surface.

To characterize the inner, the PANI/PA/CM was cut into slices to be observed with TEM images. Interestingly, the PANI loose nanoparticles (mean size were 100 nm) constituted of nanofibers which exhibited uniform 3D mesh structure, and were dispersed homogeneously in the CM from inside to outside, as shown in Fig. 2a and b. The nano-porous structure of the cellulose matrix supplied not only cavities for the *in situ* synthesis of PANI, but also a shell to protect the growing of the PANI aggregates in the microsphere. It is worth noting that in our previous work, the proportion of PANI in PANI/CNT/cellulose composite films decreases as the depth increases as a result of the slow diffusion of the aniline in the interior.[12] However, in this work, the PANI nanoparticles were homogeneously dispersed in the CM from surface to inner, owing to the doping phytic acid, which induced the uniform diffusion of the aniline in the CM, driven by the hydrogen bonds. In our findings, the phytic acid could not only connect firmly with both PANI and cellulose to create micro- and nano-porous architecture, but also acted as a doping agent of PANI. Fig. 2c and d shows the nitrogen adsorption and desorption isotherms as well as the Barrett–Joyner–Halenda (BJH) pore size distribution of the CM and PANI/PA/CM. These microspheres exhibited a type I H3 hysteresis loop according to the IUPAC and BDDT classification, as the adsorption branch was parallel to P/P_0 over a large extent. The Brunauer–Emmett–Teller (BET) surface area of the CM and PANI/PA/CM was calculated to be ~176 $m^2\ g^{-1}$ and ~152 $m^2\ g^{-1}$, respectively. The pore size distribution indicated that the PANI/PA/CM had smaller mesopores, approximately 8 nm at peak maximum (Fig. 2d). These results further confirmed the occupying of PANI in the pore of the CM, resulting in a decrease of the pore size and BET.

To further confirm the existence of strong hydrogen bonding of phytic acid with the –OH of cellulose and the –NH of PANI, the CM and PANI/PA/CM were investigated with the solid-state cross-polarization/magic-angle spinning (CP/MAS) ^{13}C NMR (Fig. 3a) and ^{13}P NMR (Fig. S4b†) spectra. The CM displayed characteristic chemical shifts at 106.1, 88.4, 75.3, and 63.3 ppm, assigning to the C1, C3, C2 and C6 of cellulose II, respectively.[18]

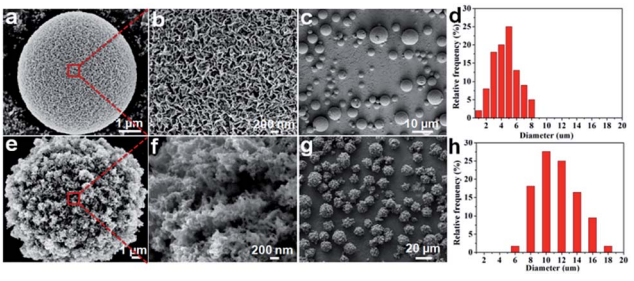

Fig. 1 SEM image of a cellulose microsphere (CM) (a); high magnification SEM image of the surface (b); SEM image (c) and histogram of the size distribution (d) of the CM; SEM image of the PANI/PA/CM (e); a high magnification SEM image of the surface (f); SEM images (g) and histogram of the size distribution (h) of the PANI/PA/CM.

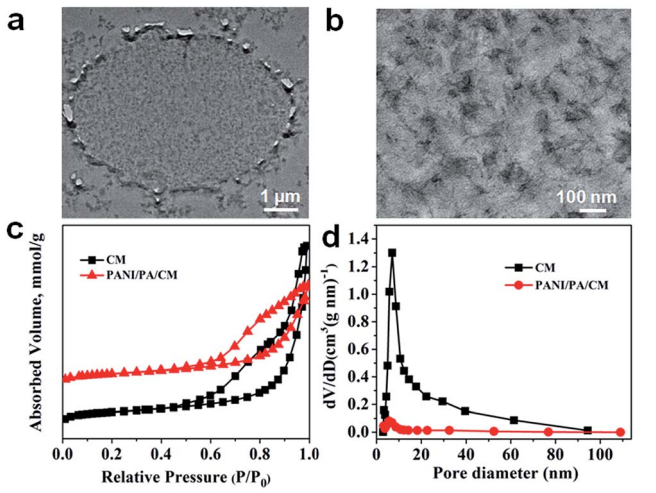

Fig. 2 TEM image of a PANI/PA/CM (a); a high magnification TEM image of inside (b); nitrogen adsorption and desorption isotherms (c) and Barrett–Joyner–Halendar (BJH) pore size distribution of cellulose microspheres (CM) and PANI/PA/CM (d).

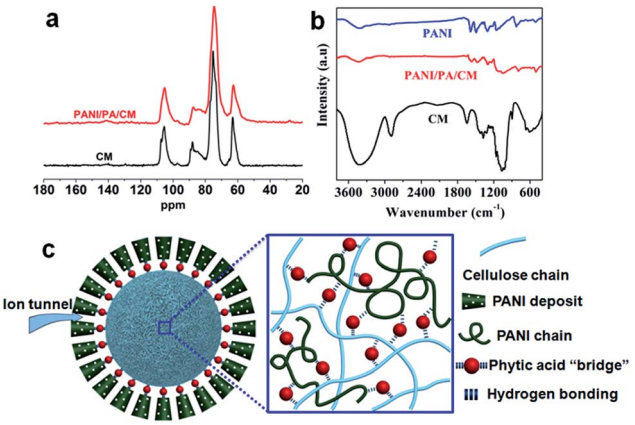

Fig. 3 Solid-state CP/MAS ^{13}C NMR spectra (a) and FT-IR spectra (b) of the PANI, PANI/PA/CM and cellulose microspheres (CM); a schematic of the PANI/PA/CM (left, c) and architecture of the hydrogen bonded PANI/PA/cellulose complex through phytic acid "bridge" (right, c).

As a result of the possible hydrogen-bond interactions between the phytic acid and the –OH of cellulose and the –NH of PANI, the chemical shifts of C2, C3 and C6 for cellulose in the PANI/PA/CM shifted to upfield by about 1 ppm and the intensity of the shoulder peak for the C4 carbon (amorphous regime) was significantly enhanced compared with the CM, suggesting the weakening of the hydrogen bonding of cellulose itself by the formation of new hydrogen bonds between the three components. Furthermore, the ^{13}P NMR spectrum of the PANI/PA/CM (Fig. S4b†) was compared with that of the pure phytic acid (Fig. S4a†).[19] There are five symmetrical signals in the ^{31}P fast-MAS NMR spectrum of the phytic acid due to the ^{31}P-D spin–spin coupling. However, the multiple signals of ^{31}P of the PANI/PA/CM became less, which could be attributed to the changed chemical environments of P atoms, indicating the presence of a strong interaction between phytic acid and cellulose and PANI. Fig. 3b shows the Fourier transform infrared (FTIR) spectroscopy of the PANI, CM and PANI/PA/CM. The peak at 3300–3500 cm^{-1} corresponds to the stretching absorption peak of O–H of cellulose, and its intensity was much weaker in the PANI/PA/CM than that in the CM, indicating that the native hydrogen bonding in cellulose was broken by the incorporation of phytic acid and PANI. The broad bands around 1304 and 1237 cm^{-1} were attributed to the characteristic C–N and C=N stretching vibration absorption peaks of PANI, respectively,[20] indicating the existence of PANI in the PANI/PA/CM. The conclusion was also supported by the results from X-ray photoelectron spectroscopy (XPS) (Fig. S5†), wide-angle X-ray diffraction (WAXD) and thermal gravimetric analysis (Fig. S6†).[21] Furthermore, the TG curves (Fig. S6†) indicated that the thermal stability of the PANI/PA/CM was higher than that of the CM, which was related to the strong hydrogen bonding interaction between phytic acid, cellulose and PANI.

On the basis of the above experimental results and theoretic analysis, a possible mechanism for the construction of the PANI/PA/CM is proposed in Fig. 3c (left). There were many nanopores of 100–200 nm in the CM, supported by the results in Fig. 1a and b. The PANI chains were immobilized in the backbones of the CM *via* the phytic acid "bridge", as shown in Fig. 3c (right) and supported by the results in Fig. 2a, b, 3a and b and S4–S6.† In our findings, the phytic acid serving as a "bridge" played an important role in the firm fixing of the PANI chains in the regenerated CM matrix through hydrogen bonds as well as the formation of the homogeneous porous architecture of the PANI/PA/CM. As shown in Fig. 3c (left), the PANI deposits on the surface of the CM formed a coralline porous architecture, supported by the results in Fig. 2a and S3c.† The PANI component with micro- and nano-porous structure could provide ion channels for the penetration of the electrolyte, whereas cellulose contributed affinity to the sulfuric acid electrolyte, which was very important in the electrode materials.

To evaluate the electrochemical performances of the PANI/PA/CM, a test was first performed in 1 M H_2SO_4 in three-electrode configurations with activated carbon as the counter electrode and Ag/AgCl as the reference electrode. The electrodes were composed of 80 wt% PANI/PA/CM, 10 wt% acetylene black (Alfa Aesar, 99.9%), and 10 wt% polytetrafluoroethylene (PTFE) as a binder to be flexible circular electrodes (Fig. S2†). In the cyclic voltammetry (CV) curves (Fig. 4a), two pairs of redox peaks were apparently displayed, which correspond to the leucoemeraldine/emeraldine and emeraldine/pernigraniline transitions of PANI, revealing the pseudocapacitance behavior of PANI. Moreover, the electrodes exhibited very fast current responses within 4 s at the switching potentials (−0.1 V and 0.7 V), which could be attributed to the high conductivity. It was worth noting that the sheet resistance of the PANI/PA/CM was measured to be 6.0–6.5 Ω sq^{-1}. The good conductivity could also be observed from the electrochemical impedance spectroscopy (EIS), as shown in Fig. 4b. A small semi-circle of about 3.5 Ω appeared in the low-frequency region, indicating a low charge transfer resistance. Moreover, the EIS of pure PANI was about

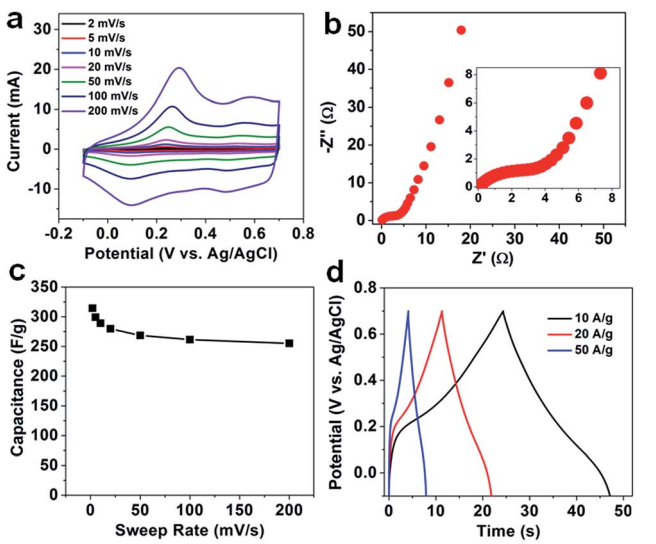

Fig. 4 Electrochemical performances in three-electrode configurations: CV curves of PANI/PA/CM electrode with a sweep rate from 2 to 200 mV s^{-1} (a); EIS spectrum (b); capacitance *versus* sweep rate (c); GCD curves under high current density of 10, 20 and 50 A g^{-1} (d). The inset shows the charge transfer resistance.

12.5 Ω (Fig. S7†), which was larger than that of PANI/PA/CM. Considering that charge transfer resistance is a combination of electron and ion conductivity, both the PANI/PA/CM structure and the nanopores contributed to this good performance of the PANI/PA/CM. Firstly, the superior affinity between cellulose and the electrolyte ensured that the PANI/PA/CM served as a reservoir, adsorbing large amount of ions around the electrodes. Secondly, the micro- and nano-porous architecture of the PANI/PA/CM could facilitate the permeation of the ions, accelerating the ion diffusion. Finally, the coralline PANI deposits on the surface and the inner mesh structure of the PANI/PA/CM provided a stable tunnel for fast proton transport. It is expected that this material could provide excellent power handling properties, which is the most important feature of supercapacitors. To demonstrate our hypothesis, the curve of capacitance *versus* sweep rate is shown in Fig. 4c, which was obtained *via* the equation: $\int(IV)/(mv\Delta V)$ from the CV curves in Fig. 4b. At a low sweep rate of 2 mV s^{-1}, the specific capacitance was 314 F g^{-1}, and at a low current density of 1.1 A g^{-1}, the specific capacitance was 349 F g^{-1} in the curve of capacitance *versus* current density (Fig. S8†). These results indicated the good specific capacitance of PANI/PA/CM. Surprisingly, at a high sweep rate of 200 mV s^{-1} (charge/discharge time of 4 s), the capacitance was still 255 F g^{-1}, which was 81.2% retention of the capacitance from 2 to 200 mV s^{-1}. Such a high rate capability was superior to that of the most recently reported PANI/carbon composite electrode, such as PANI/graphene composite paper (64.2% of capacitance retention with the current density increase from 1 A g^{-1} to 10 A g^{-1}) and PANI coated on graphitized carbon nanofibers (52% capacitance retention with the current density increased from 0.4 A g^{-1} to 50 A g^{-1}). Given that cellulose makes no contribution to the capacitance due to the insulation, and the mass loading of PANI was not low (~1 mg cm^{-2}), such an excellent rate capability could only be attributed to the featured porous structure, the affinity between cellulose and electrolyte, and the hydrogen bonded "bridge". The high rate properties could also be testified by galvanostatic charge–discharge (GCD) tests. As shown in Fig. 4d, the GCD curves were almost symmetric and even displayed a small *IR* drop at a high current density of 50 A g^{-1}.

For application consideration, a two-electrode setup measurement is of more significance. Here, a device was fabricated by sandwiching two identical electrodes with a separator, and the electrolyte was still 1 M H_2SO_4. From the normalized CV curves shown in Fig. 5a, the area of CV curves hardly changed, suggesting a good rate capability. GCD curves from 0.5 to 20 A g^{-1} are shown in Fig. 5b. From the symmetric profiles with a small *IR* drop in the GCD curves, the PANI/PA/CM electrodes exhibited good conductivity. Fig. 5c shows the gravimetric capacitance under the sweep rate from 2 to 100 mV s^{-1}. At a low sweep rate of 2 mV s^{-1}, the gravimetric capacitance was only 65 F g^{-1}. Similarly, with the three-electrode measurement, the device revealed an excellent rate capability with 70% capacitance retention. In addition, the highest energy density is 5.8 W h kg^{-1} with a power density of 130 W kg^{-1}. Importantly, the device could deliver a high power density of 1783 W kg^{-1} with an energy density of 4 W h kg^{-1} (Fig. S9†).

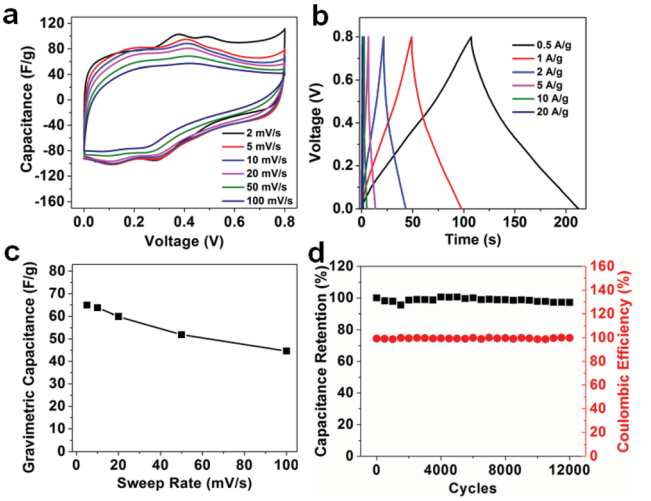

Fig. 5 Electrochemical performance for a two-electrode device with PANI/PA/CM films as the electrodes: normalized CV curves under a sweep rate from 2 to 100 mV s^{-1} (a); GCD curves under current density from 0.5 to 20 A g^{-1} (b); capacitance *versus* sweep rate (c); cycling stability and coulombic efficiency for 12 000 cycles under 2 mA (d).

Since the first invention of PANI,[22] the constraint of its industrial application is its poor cycling stability. The swelling and contraction of PANI during charging/discharging, which results in the fracture of PANI chains, is the main reason for the cycling degradation. Here, in our findings, a very strong and tough connection between PANI and cellulose provided by the phytic acid "bridge", and the micro- and nano-porous structure led to the electrochemical stability of PANI. As shown in Fig. 5d, no apparent degradation of PANI could be observed after 12 000 cycles with high coulombic efficiency of around 100%. This excellent cycling stability of PANI/PA/CM was much better than the common values of PANI or PANI/carbon composite electrodes, (Table S1†) and the cycling stable capability was higher by 12 times than that of PANI/CNT/cellulose films in our previous work.[14] Yushin *et al.*[23] have reported an excellent PANI/multifunctional CNT composite electrode with stability of 30 000 cycles, which needed an additive multifunctional CNT as the scaffold. In our findings, the PANI/PA/CM based device without any inorganic additives had excellent cycling stability, high rate capability and good conductivity. This could be owing to the unique role of the hydrogen bonded phytic acid "bridge". By virtue of the low cost and easy synthesis procedure, it is reasonable to expect that the PANI/PA/CM electrodes have both scientific and industrial merits.

In summary, PANI was *in situ* synthesized in regenerated cellulose microspheres, which were prepared from cellulose in LiOH/urea aqueous solution, to construct novel PANI/PA/CM electrode materials with phytic acid as the "bridge". The PANI/PA/CM successfully resolved the problem of the pulverization of PANI to be used as electrode materials. The phosphorus oxygen groups in the phytic acid could form strong hydrogen bonding with both the cellulose and the PANI, firmly fixing the PANI chains on the cellulose template. The PANI subparticles with

nanomesh structure were dispersed homogeneously in the cellulose microspheres from inside to outside, as a result of the firm connection between hydrophobic PANI and hydrophilic cellulose through hydrogen bonds to create micro- and nano-porous architecture. The other part of PANI deposited on the surface of the microspheres to form a loose coralline structure, leading to good ion channels for the penetration of the electrolyte. The PANI/PA/CM exhibited excellent cycling stability (over 12 000 cycles), high rate capability and good conductivity as an electrode material. The superior affinity of cellulose with the electrolyte, the homogeneous micro- and nano-porous architecture, and the large specific surface area of the PANI/PA/CM played an important role in achieving such a high electrochemical performance. This work provided a novel, large-scale and cost-efficient strategy to construct highly efficient electrode materials, which will have potential applications in energy storage.

Acknowledgements

This work was financially supported by the National Basic Research Program of China (973 Program, 2010CB732203), the Major Program of National Natural Science Foundation of China (21334005), and the Natural Science Foundation of China (51322210, 61434001, and 21422405). The authors express thanks for the support of the Center for Nanoscale Characterization & Devices (CNCD), WNLO-HUST and the Analysis and Testing Center of Huazhong University of Science and Technology.

Notes and references

1 (*a*) J. E. Trancik, *Nature*, 2014, **507**, 300; (*b*) H. Williams, A. De Benedictis, R. Ghanadan, A. Mahone, J. Moore, W. R. Morrow III, S. Price and M. S. Torn, *Science*, 2012, **335**, 53; (*c*) N. Armaroli and V. Balzani, *Angew. Chem., Int. Ed.*, 2007, **46**, 52; (*d*) M. Carbajales-Dale, C. J. Barnhart and S. M. Benson, *Energy Environ. Sci.*, 2014, **7**, 1538.

2 (*a*) P. Simon and Y. Gogotsi, *Nat. Mater.*, 2008, **7**, 845; (*b*) X. L. Wu, L. Y. Jiang, F. F. Cao, Y. G. Guo and L. J. Wan, *Adv. Mater.*, 2009, **21**, 2710; (*c*) Y. Yang, H. Fei, G. Ruan, C. Xiang and J. M. Tour, *Adv. Mater.*, 2014, **26**, 8163.

3 (*a*) D. Ge, L. Yang, L. Fan, C. Zhang, X. Xiao, Y. Gogotsi and S. Yang, *Nano Energy*, 2015, **11**, 568; (*b*) Y. Yang, Y. Hao, J. Yuan, L. Niu and F. Xia, *Carbon*, 2014, **78**, 279; (*c*) W. Zhou, Y. Yu, H. Chen, F. J. Disalvo and H. D. Abruna, *J. Am. Chem. Soc.*, 2013, **135**, 16736; (*d*) S. Li, D. Huang, J. Yang, B. Zhang, X. Zhang, G. Yang, M. Wang and Y. Shen, *Nano Energy*, 2014, **9**, 309.

4 (*a*) S. Giri, D. Ghosh and C. K. Das, *Adv. Funct. Mater.*, 2014, **24**, 1312; (*b*) D. Vonlanthen, P. Lazarev, K. A. See, F. Wudl and A. J. Heeger, *Adv. Mater.*, 2014, **26**, 5095.

5 M. Yu, Y. Ma, J. Liu and S. Li, *Carbon*, 2015, **87**, 98.

6 T. Liu, L. Finn, M. Yu, H. Wang, T. Zhai, X. Lu, Y. Tong and Y. Li, *Nano Lett.*, 2014, **14**, 2522.

7 (*a*) S. Li, D. Wu, C. Cheng, J. Wang, F. Zhang, Y. Su and X. Feng, *Angew. Chem., Int. Ed.*, 2013, **52**, 12105; (*b*) C. Lu, T. Ben, S. Xu and S. Qiu, *Angew. Chem., Int. Ed.*, 2014, **53**, 6454; (*c*) J. Zang and X. Li, *J. Mater. Chem.*, 2011, **21**, 10965; (*d*) X. Zhang, X. Zeng, M. Yang and Y. Qi, *ACS Appl. Mater. Interfaces*, 2014, **6**, 1125.

8 (*a*) H. Wang, G. Gurau and R. D. Rogers, *Chem. Soc. Rev.*, 2012, **41**, 1519; (*b*) S. Zhu, Y. Wu, Q. Chen, Z. Yu, C. Wang, S. Jin, Y. Ding and G. Wu, *Green Chem.*, 2006, **8**, 325.

9 (*a*) C. M. Cirtiu, A. F. Dunlop-Brière and A. Moores, *Green Chem.*, 2011, **13**, 288; (*b*) Z. Gui, H. Zhu, E. Gillette, X. Han, G. W. Rubloff, L. Hu and S. Lee, *ACS Nano*, 2013, **7**, 6037; (*c*) S. Dong and M. Roman, *J. Am. Chem. Soc.*, 2007, **129**, 13810; (*d*) M. M. Malinen, L. K. Kanninen, A. Corlu, H. M. Isoniemi, Y. R. Lou, M. L. Yliperttula and A. O. Urtti, *Biomaterials*, 2014, **35**, 5110; (*e*) R. J. Moon, A. Martini, J. Nairn, J. Simonsen and J. Youngblood, *Chem. Soc. Rev.*, 2011, **40**, 394; (*f*) L. Zhang, Z. Liu, G. Cui and L. Chen, *Prog. Polym. Sci.*, 2015, **43**, 136.

10 (*a*) S. Li, D. Huang, B. Zhang, X. Xu, M. Wang, G. Yang and Y. Shen, *Adv. Energy Mater.*, 2014, **4**, 1; (*b*) C. Long, D. Qi, T. Wei, J. Yan, L. Jiang and Z. Fan, *Adv. Funct. Mater.*, 2014, **24**, 3953; (*c*) H. Wang, L. Bian, P. Zhou, J. Tang and W. Tang, *J. Mater. Chem. A*, 2013, **1**, 578.

11 (*a*) X. Shi, L. Zhang, J. Cai, G. Cheng, H. Zhang, J. Li and X. Wang, *Macromolecules*, 2011, **44**, 4565; (*b*) X. Shi, Y. Hu, K. Tu, L. Zhang, H. Wang, J. Xu, H. Zhang, J. Li, X. Wang and M. Xu, *Soft Matter*, 2013, **9**, 10129; (*c*) X. Shi, Y. Hu, F. Fu, J. Zhou, Y. Wang, L. Chen, H. Zhang, J. Li, X. Wang and L. Zhang, *J. Mater. Chem. A*, 2014, **2**, 7669.

12 (*a*) X. Luo, S. Liu, J. Zhou and L. Zhang, *J. Mater. Chem.*, 2009, **19**, 3538; (*b*) J. Duan, X. He and L. Zhang, *Chem. Commun.*, 2015, **51**, 338.

13 Z. Shi, H. Gao, J. Feng, B. Ding, X. Cao, S. Kuga, Y. Wang, L. Zhang and J. Cai, *Angew. Chem., Int. Ed.*, 2014, **53**, 5380.

14 X. Shi, Y. Hu, M. Li, Y. Y. Duan, Y. Wang, L. Chen and L. Zhang, *Cellulose*, 2014, **21**, 2337.

15 (*a*) L. Pan, G. Yu, D. Zhai, H. R. Lee, W. Zhao, N. Liu, H. Wang, B. C.-K. Tee, Y. Shi, Y. Cui and Z. Bao, *Proc. Natl. Acad. Sci. U. S. A.*, 2012, **109**, 1; (*b*) B. Liu, P. Soares, C. Checkles, Y. Zhao and G. Yu, *Nano Lett.*, 2013, **13**, 3414; (*c*) L. Pan, A. Chortos, G. Yu, Y. Wang, S. Isaacson, R. Allen, Y. Shi, R. Dauskardt and Z. Bao, *Nat. Commun.*, 2014, **5**, 1; (*d*) H. Wu, G. Yu, L. Pan, N. Liu, M. T. McDowell, Z. Bao and Y. Cui, *Nat. Commun.*, 2013, **4**, 1; (*e*) J. F. Mike and J. L. Lutkenhaus, *ACS Macro Lett.*, 2013, **2**, 839; (*f*) Y. Zhao, B. Liu, L. Pan and G. Yu, *Energy Environ. Sci.*, 2013, **6**, 2856.

16 J. Sun, X. Zhao, W. Illeperuma, O. Chaudhuri, D. Mooney, J. Vlassak and Z. Suo, *Nature*, 2012, **489**, 133.

17 J. Cai and L. Zhang, *Macromol. Biosci.*, 2005, **5**, 539.

18 Q. Wang, J. Cai, L. Zhang, M. Xu, H. Cheng, C. C. Han, S. Kuga, J. Xiao and R. Xiao, *J. Mater. Chem. A*, 2013, **1**, 6678.

19 G. Mali, M. Sala, I. Arcon, V. Kaucic and J. Kolar, *J. Phys. Chem. B*, 2006, **110**, 23060.

20 X. Li, Y. Liu, W. Guo, J. Chen, W. He and F. Peng, *Electrochim. Acta*, 2014, **135**, 550.

21 (*a*) Y. Zhu, D. Hu, M. X. Wan, L. Jiang and Y. Wei, *Adv. Mater.*, 2007, **19**, 2092; (*b*) M. Kim, C. Lee and J. Jang, *Adv. Funct. Mater.*, 2014, **24**, 2489; (*c*) C. H. B. Silva, A. M. Da Costa

Ferreira, V. R. L. Constantino and M. L. A. Temperini, *J. Mater. Chem. A*, 2014, **2**, 8205.
22 A. G. Macdiarmid, J. C. Chiang and A. F. Richter, *Synth. Met.*, 1987, **18**, 285.
23 J. Benson, I. Kovalenko, S. Boukhalfa, D. Lashmore, M. Sanghadasa and G. Yushin, *Adv. Mater.*, 2013, **25**, 6625.